Journal of Structural Geology 36 (2012) 71–80

Contents lists available at SciVerse ScienceDirect

Journal of Structural Geology

journal homepage: www.elsevier.com/locate/jsg

Fault-slip accumulation in an active rift over thousands to millions of years and the importance of paleoearthquake sampling

Vasiliki Mouslopoulou [a,b,*], Andrew Nicol [c], John J. Walsh [a], John G. Begg [c], Dougal B. Townsend [c], Dionissios T. Hristopulos [b]

[a] Fault Analysis Group, School of Geological Sciences, University College Dublin, Dublin 4, Ireland
[b] Department of Mineral Resources Engineering, Technical University of Crete, 73100 Chania, Crete, Greece
[c] GNS Science, PO Box 30368, Lower Hutt, New Zealand

ARTICLE INFO

Article history:
Received 11 May 2011
Received in revised form
1 November 2011
Accepted 17 November 2011
Available online 1 December 2011

Keywords:
Rift
Paleoearthquakes
Fault trenching
Seismic-reflection data
Fault growth
Seismic hazard

ABSTRACT

The catastrophic earthquakes that recently (September 4th, 2010 and February 22nd, 2011) hit Christchurch, New Zealand, show that active faults, capable of generating large-magnitude earthquakes, can be hidden beneath the Earth's surface. In this article we combine near-surface paleoseismic data with deep (<5 km) onshore seismic-reflection lines to explore the growth of normal faults over short (<27 kyr) and long (>1 Ma) timescales in the Taranaki Rift, New Zealand. Our analysis shows that the integration of different timescale datasets provides a basis for identifying active faults not observed at the ground surface, estimating maximum fault-rupture lengths, inferring maximum short-term displacement rates and improving earthquake hazard assessment. We find that fault displacement rates become increasingly irregular (both faster and slower) on shorter timescales, leading to incomplete sampling of the active-fault population. Surface traces have been recognised for <50% of the active faults and along ≤50% of their lengths. The similarity of along-strike displacement profiles for short and long time intervals suggests that fault lengths and maximum single-event displacements have not changed over the last 3.6 Ma. Therefore, rate changes are likely to reflect temporal adjustments in earthquake recurrence intervals due to fault interactions and associated migration of earthquake activity within the rift.

1. Introduction

Many faults grow uniformly over hundreds of thousands to millions of years by accumulating slip during large-magnitude earthquakes (Stein et al., 1988; Walsh and Watterson, 1988; Cowie and Scholz, 1992; Nicol et al., 1997, 2005a; Mouslopoulou et al., 2009) (Fig. 1). This uniformity appears to be inconsistent with the dramatic fluctuations in displacement accumulation on individual faults often observed over timescales that range from a few days (Dieterich, 1994; Kagan, 1994; Mouslopoulou and Hristopulos, 2011) to tens of thousands of years (Schwartz and Coppersmith, 1984; Lindvall et al., 1989; Marco et al., 1996; Weldon et al., 2004; Nicol et al., 2006) (Fig. 1). These variations are thought to result from the highly nonlinear nature of earthquake process, the temporal non-homogeneity of fault strength and the interactions between adjacent faults, factors which often lead to sampling biases (Zoback, 2000; Nicol et al., 2006, 2009; Dolan et al., 2007; Mouslopoulou et al., 2009; Li et al., 2009; Mouslopoulou and Hristopulos, 2011).

Analysis of active faulting at, or near, the ground surface may provide a useful, yet incomplete, earthquake history of individual faults. This is particularly true for faults with low displacement rates (<0.5 mm/yr), where the time-window of observation is similar to, or less than, the time intervals between large earthquakes on these faults. Even in circumstances where the time interval of observation is large compared with the average earthquake recurrence interval, the paleoearthquake record captured will include a randomly sampled sequence of earthquakes on a particular fault, which may not reveal whether the timing and size of these earthquakes sufficiently characterises the long-term average behaviour of the fault or the occurrence of future earthquakes. In order to assess to what extent a randomly sampled paleoearthquake record is representative of the long-term fault behaviour, fault parameters (e.g., displacement rate, recurrence

* Corresponding author. Department of Mineral Resources Engineering, Technical University of Crete, 73100 Chania, Crete, Greece. Tel.: +30 28210 37679; fax: +30 28210 37853.
E-mail address: vasiliki@mred.tuc.gr (V. Mouslopoulou).

0191-8141/$ – see front matter © 2011 Elsevier Ltd. All rights reserved.
doi:10.1016/j.jsg.2011.11.010

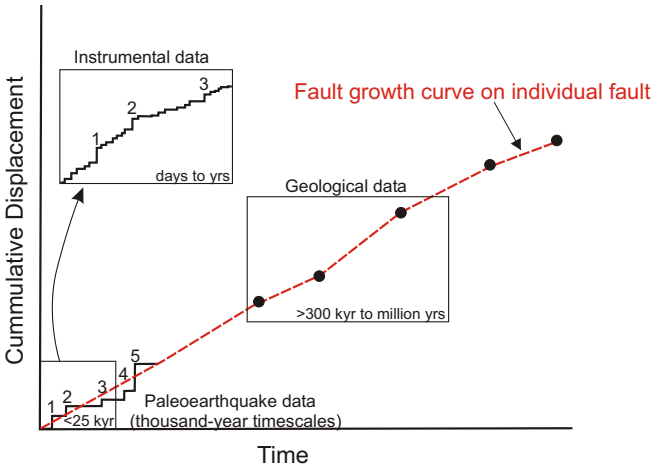

Fig. 1. Schematic diagram illustrating fault-slip accumulation over instrumental (days to yrs), paleoearthquake (e.g., <25 kyr) and geological (e.g., >300 kyr) timescales. Numbered steps in the paleoearthquake data represent large ground-surface rupturing earthquakes while steps in the day-to-year long data represent small-sized instrumentally recorded earthquakes (most of which have not ruptured the Earth's surface). Earthquakes occur with both variable slip and recurrence interval. Data resolution increases with decreasing timescales.

interval) that derive from the same fault must be compared over short- (e.g., <27 kyr) and long-term (>1 Ma) timescales (Mouslopoulou et al., 2009; Nicol et al., 2009). Specifically, assessing whether the paleoearthquake data reflect a period of accelerated earthquake activity (e.g., earthquake clustering), a period of unusually low activity (seismic quiescence) or whether the sampled record reflects the fault's average growth pattern is important, and may have implications for earthquake hazard assessment (Fig. 1).

Characterising a small fraction (e.g., <20 kyr) of the growth history of a single fault is common (e.g., Schwartz and Coppersmith, 1984; Rockwell et al., 2000; Weldon et al., 2004; Palumbo et al., 2004; Nicol et al., 2006; Schlagenhauf et al., 2011); assessing, however, both its short- (<27 kyr) and long-term (>1 Ma) growth patterns is rare. Capturing the growth history of faults over short and long time intervals requires stratigraphic preservation of fault-slip in well dated sequences and also the use of multiple field techniques (e.g. fault trenching, outcrop geology and seismic-reflection lines). Preservation of syn-sedimentary growth strata is only achieved in circumstances where little erosion has taken place and sedimentation rates are greater than or equal to vertical displacement rates. In such cases, past large-magnitude ($M > 5.5$) earthquakes will be recorded in the stratigraphy. Whilst the resolution of this record decreases for increasing timescales, with individual earthquakes mainly being distinguishable over the last ca. 50 kyr (e.g., Marco et al., 1996), the cumulative effect of 100's to 1000's of earthquakes will be recorded by displacements of 100's to 1000's of metres on stratigraphic markers (Fig. 1).

The Taranaki Rift, New Zealand, provides a unique opportunity to quantify and compare displacements accumulated on individual normal faults over timescales that range from individual earthquakes to millions of years. In this paper, we compare high-quality trench (short-term) and seismic-reflection (long-term) data for faults in the rift. This information has been used to examine sampling biases in the short-term (<27 kyr) data and to consider their implications for seismic hazard assessment. Results show that active faults that displace the ground surface by $<\sim 1$ m are not routinely resolved, resulting in underestimation of fault lengths by up to 85% and incomplete temporal and spatial sampling of paleoearthquakes on faults with short-term displacement rates of <0.14 mm/yr. Consequently, short-term fault data generally overestimate average long-term displacement rates on surface-rupturing faults, while they underestimate their earthquake recurrence intervals and total fault lengths. Short-term data also underestimate the total number of active faults in the system and, thus, the local seismic hazard.

2. Geological setting and fault data

The Taranaki Rift extends for about 350 km within the Taranaki Basin, which is mainly west of the North Island of New Zealand (Fig. 2, inset) (Townsend et al., 2010). The rift is part of a back-arc basin, forming in association with subduction of the Pacific Plate beneath the Australian Plate along the Hikurangi margin (Fig. 2, inset) (Walcott, 1987; King and Thrasher, 1996; Wallace et al., 2004; Giba et al., 2010). Extension may reflect regional processes, including clockwise rotation of the North Island and slab roll-back along the Hikurangi margin.

The Taranaki Rift traverses the Taranaki Peninsula where it comprises multiple active-fault traces at the ground surface that strike NE–SW (Fig. 2). The rift is 30–50 km wide and accommodates extension rates of 1–2 mm/yr. Faulting and fault-related extension die out laterally towards the north-east of the peninsula, with the associated transfer of displacement onto faults to the northwest within the offshore Taranaki Basin (Fig. 2, inset). The present rifting phase commenced in the Pliocene (3–4 Ma) and has produced, over different temporal scales and across a range of earthquake magnitudes, kilometre-scale cumulative displacements on normal faults (Nicol et al., 2005a, 2007; Giba et al., 2010; this study), active faulting at the ground surface (Hull, 1994; Townsend et al., 2008, 2010; this study) and historical seismicity (Robinson et al., 1976; Reyners, 1989; Hull, 1994; Downes, 1995; Sherburn and White, 2005, 2006).

Crustal extension on the Taranaki Peninsula is also associated with widespread late Quaternary (≤0.57 Ma) volcanism (Alloway et al., 2005). The most recent phase of volcanic activity started about 100 kyr (last eruption ca. 250 years ago) and resulted in the formation of the impressive volcanic cone of Mt. Taranaki. Although Mt. Taranaki rises to 2518 m above sea-level (a.s.l.) and dominates the landscape, studies presently show no clear link between the timing of prehistoric large-magnitude earthquakes in the rift and volcanic eruptions or episodes of cone collapse (Giba, 2010; Townsend et al., 2010).

In this paper, we combine seismic-reflection and trench data from individual faults to chart their displacement accumulation through time. Two-dimensional (2D) seismic-reflection lines extend southwest of Mt. Taranaki, across the entire onshore width of the rift and in a rift-parallel direction for about 20 km (Fig. 2). The 2D seismic survey comprises a total of 21 fault-perpendicular and 17 fault-parallel lines spaced at 0.5–5 km. These lines image all of the known active faults and provide estimates of ≥0.5 Ma cumulative throws (i.e. vertical displacements) at each of ten trench sites. Faulted subsurface seismic reflectors imaged to depths of up to ca. 5 km have been tied to five wells (Figs. 2 and 3a) in which the stratigraphy was dated using micropalaeontology (King and Thrasher, 1996). The six youngest of these seismic reflectors (ca. 0.5, 2.7, 3, 3.6, 5.5 and 10 Ma) were traced along and across the faults throughout the grid of seismic lines and provide information on the growth of fault displacement during the Plio-Pleistocene. These vertical displacements range, on individual faults, up to ca. 1.5 km and decrease with reduction in horizon age from 3.6 Ma (Fig. 3a).

To constrain the paleoearthquake history of the six active faults with resolvable surface traces, 10 trenches have been excavated. Trench data provide information for a total of 23 large

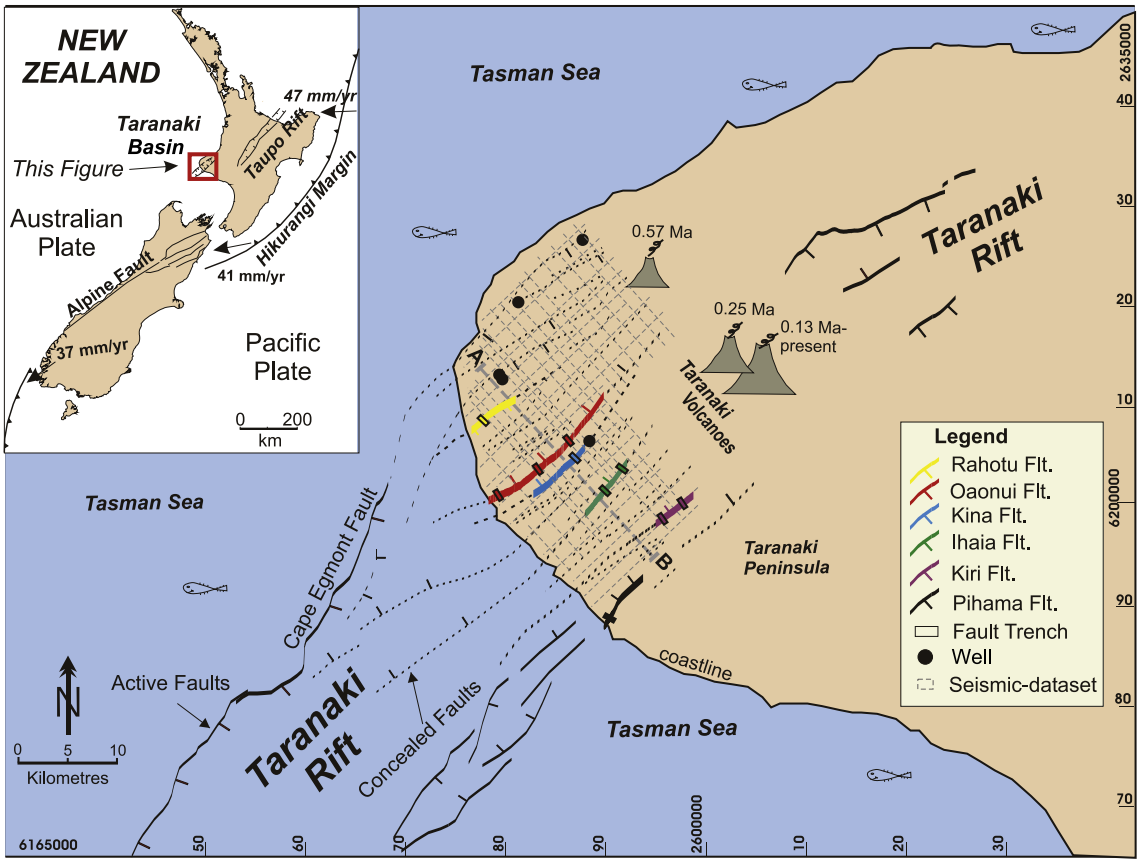

Fig. 2. Fault map of the Taranaki Rift in the area adjacent to Taranaki Peninsula. Onshore faults that rupture the ground surface are colour-coded (numbered in printed version) and offshore faults that rupture the sea-floor are indicated with black solid lines. Concealed faults are indicated with black dashed lines. The seismic-reflection lines and the five wells are indicated with grey dashed lines and black filled circles, respectively. The localities of the fault-trenches are indicated by the black rectangles. Late Quaternary to present volcanic activity on the peninsula is highlighted. Surface fault traces northeast of the volcanoes define the northeastward termination of this part of the Taranaki Rift. Inset: the study area is located on the North Island of New Zealand, to the east of which the Pacific Plate is being subducted beneath the Australian Plate along the Hikurangi margin.

paleoearthquakes that ruptured the ground surface during the last 27 kyr (Fig. 3b). These surface-rupturing earthquakes are a sub-sample of the entire population, with events <M5.5 considered unlikely to be routinely recorded in the trench data (see McCalpin, 2009). The earthquake record is complete for the last 5 kyr on all six active faults and for 27 kyr on two of these faults (Fig. 7a). Vertical displacements measured in the trenches range from 0.1 m to 4 m (e.g., Townsend et al., 2010; Fig. 3b). These displacements accrued during earthquakes with single-event displacements of up to 1.2 m (Townsend et al., 2010). They represent point measurements on fault traces (accrued during one or more earthquakes) and have been supplemented by scarp height measurements recorded along the length of each active trace. The age of paleoearthquakes is primarily constrained by ^{14}C dating of near-surface (<6 m deep) stratigraphy displaced by the faults (Neall and Alloway, 2004; Townsend et al., 2010 and references therein) (Fig. 3b). The available horizon ages and displacement measurements produce displacement rates for each timescale that range up to ±30% and are significantly less than the variations in displacement rates observed for individual faults in the system. For further details of the trenching and the paleoearthquake history on each fault see Townsend et al. (2010).

3. Fault displacements and lengths

Seismic-reflection and outcrop (including trench) data have been used to chart temporal and spatial changes in vertical displacements and fault lengths, for all resolvable faults in the rift. Seismic-reflection lines onshore southwest of Mt. Taranaki (Fig. 2) reveal that the rift comprises a total of 47 northeast–southwest striking normal faults with lengths of 2–30 km and maximum displacements of 20 m to 1.5 km (Figs. 4a and 5b). The rift comprises approximately equal numbers of southeast ($N = 21$) and northwest ($N = 26$) dipping faults (Fig. 4a).

The available seismic-reflection lines record many more faults than those inferred from field mapping of their active traces. Thirteen faults clearly displace the 0.5 Ma horizon and extend upwards above this horizon towards the ground surface (Fig. 3b). It is a distinct possibility that additional faults also displace the 0.5 Ma horizon but have displacements that are below the ~20 m resolution of the seismic-reflection data. Interpretation of aerial ortho-photographs and field mapping suggest that six of these faults have surface scarps up to 4 m high and displace a diachronous landscape mainly ranging in age from ~8 to 27 kyr (Fig. 2) (Townsend et al., 2010). Trenching confirms that these faults are active and have ruptured the ground surface during prehistoric large-magnitude earthquakes (Figs. 3b and 4b) (Townsend et al., 2010). The remaining seven faults that displace the 0.5 Ma horizon, most of which are large (>1000 m of cumulative throw), also displace near-surface horizons (<50 m below the ground surface), but have no resolvable surface trace and probably last ruptured within the last 100–200 kyr (Fig. 3a). These faults are probably active and capable of generating future large-magnitude earthquakes (see discussion in the following section).

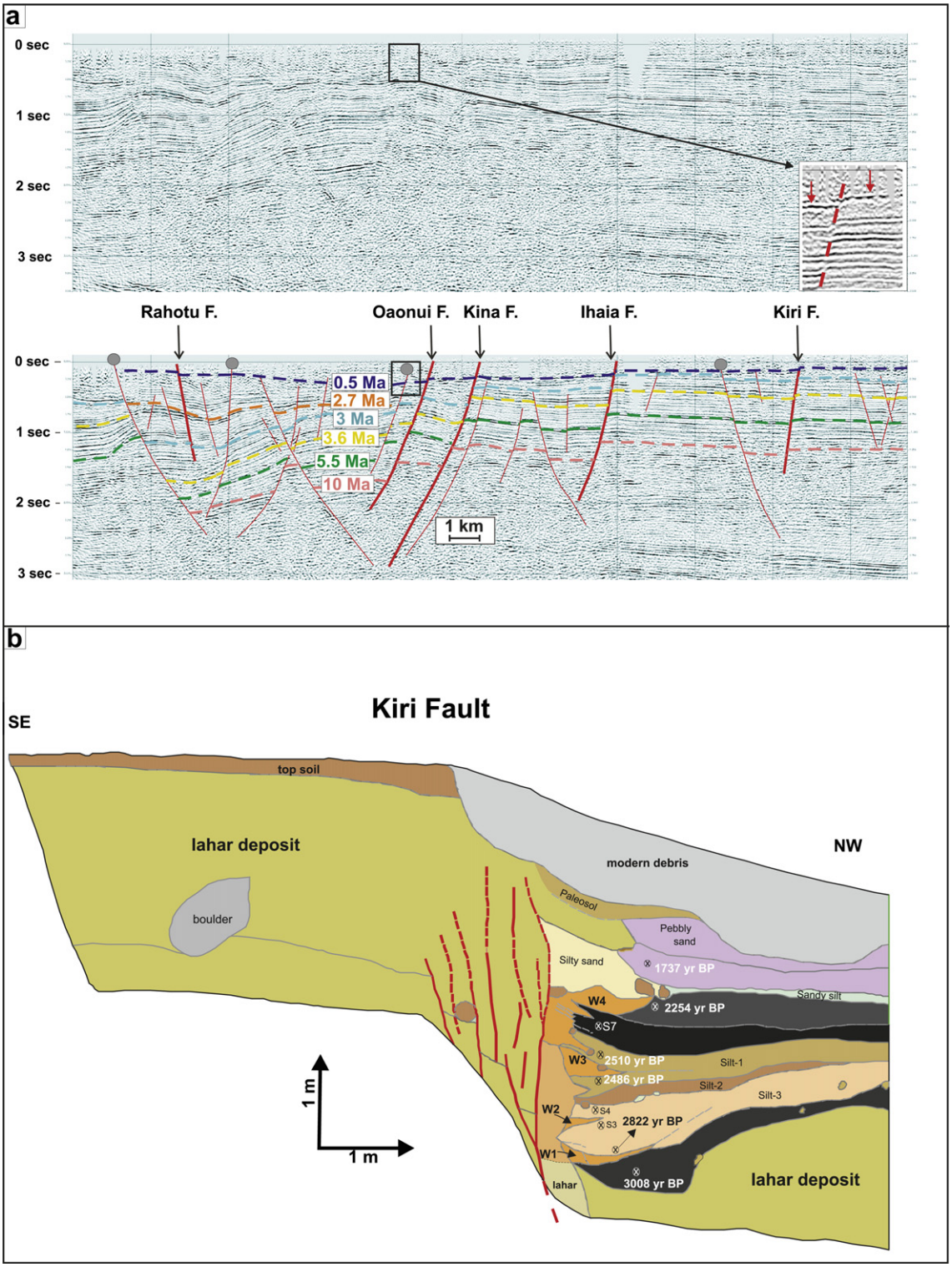

Fig. 3. a) Uninterpreted (above) and interpreted (below) seismic-reflection profile across the transect A–B (for location see Fig. 2). Twenty-four normal faults are identified to displace up to six horizons of 0.5–10 Ma in age. The active faults with surface traces and inferred active faults that displace the 0.5 Ma horizon are indicated by arrows and grey circles, respectively. Depth is in two-way-traveltime (TWT) seconds. Time to depth conversions derived from well-ties extending down to 2.5 s ($y = 1.5807x - 260.09$). Inset: Fault displacing post-0.5 Ma horizon (indicated by arrows). b) Example of trench-log from the Kiri Fault, which has been the fastest moving fault in the Taranaki Rift during the Holocene. From the trench-log five earthquakes are inferred to have ruptured the ground surface during the last 3 kyr (see formation of successive colluvial wedges 'W_i'). The timing of the earthquakes is constrained by nine radiocarbon (^{14}C) ages.

Fault lengths in the subsurface are generally much longer than their equivalent surface trace lengths. Trace lengths for the six active faults range from 1.4 (Rahotu Fault) to 13.2 km (Oaonui Fault), while their subsurface lengths are between 20 and 30 km (Fig. 4; Tables 1 and 2). Analysis of individual faults suggests that the subsurface fault lengths are about 2–8 times larger than their equivalent surface traces (Fig. 4c). Some of this discrepancy arises because fault scarps <1 m in height are typically sub-resolution,

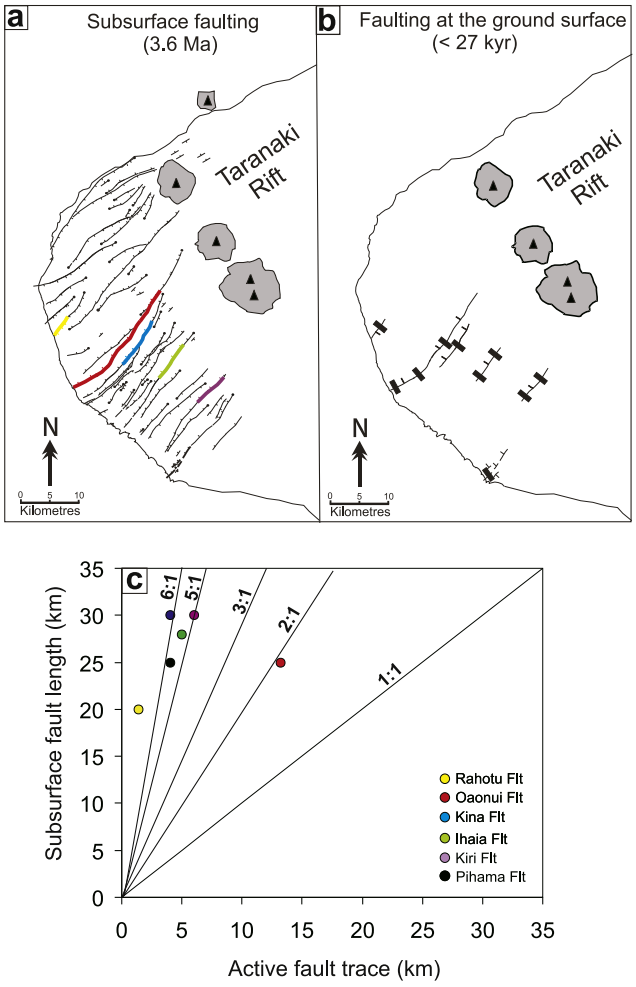

Fig. 4. Fault maps for the onshore Taranaki Rift showing faults that displace the 3.6 Ma horizon (a) and the ground surface (< 27 kyr) (b). Subsurface faulting is imaged on seismic-reflection profiles, down to depths of 5 km. Colour-coded (numbered in printed version) active-fault traces are superimposed onto the 3.6 Ma fault map for comparison. Active faults are those that displace the ground surface by more than ca. 1 m; those with ground surface displacements of less than 1 m are not routinely resolved resulting in significant underestimates of fault lengths. Late Quaternary to Recent volcanic activity on the peninsula is highlighted. (c) Plot comparing the surface and subsurface fault lengths on each of the six active faults. Length of active traces are severely underestimated. See text for discussion.

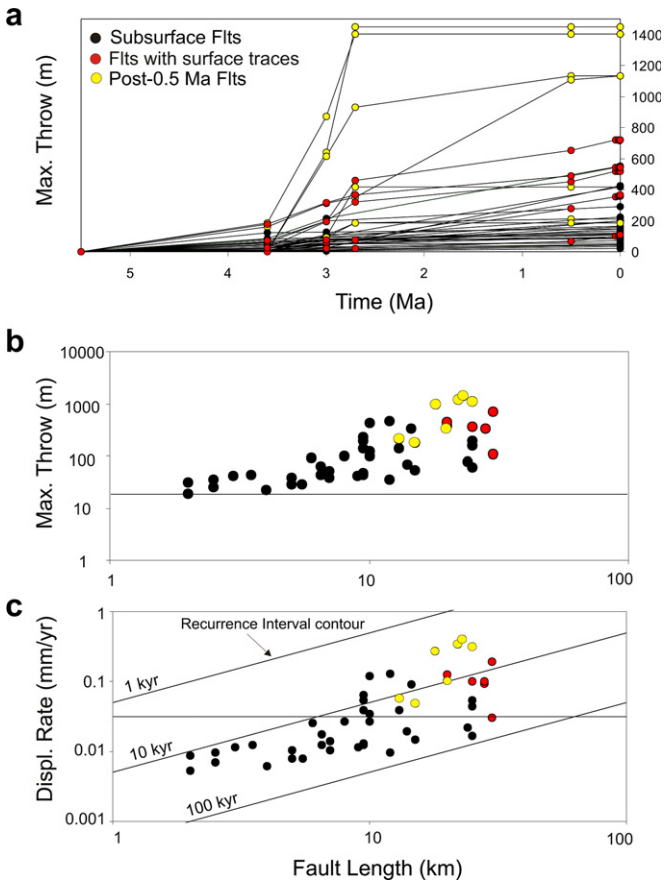

Fig. 5. a) Throw vs. time plot illustrating the long-term (0–5.5 Ma) accumulation of vertical displacement (at the point of maximum throw) on the 47 faults in the system; b) and c) Log–log plots illustrating the maximum throw and throw rate, calculated over the last 3.6 Ma for each fault in the rift, as a function of fault length. Contours of earthquake recurrence interval are estimated from the standard slip/length relationship for earthquakes (i.e. $De = 0.00005^{*}L$, where De is the slip during an earthquake and L is the fault length; Wells and Coppersmith, 1994), assuming the superimposition of characteristic earthquakes with maximum earthquake-slip. The faults that rupture the ground surface and those that rupture the 0.5 Ma horizon (but not the ground surface) are indicated (see key in 5a). Horizontal grey lines in (b) and (c) indicate resolution limit for seismic datasets (ca. 20 m) and outcrop mapping (ca. 1 m, which over 27 kyr produces slip rates of ca. 0.03 mm/yr), respectively.

particularly in areas where local topography is in excess of 1 m, resulting in undersampling of these low fault scarps (for further discussion see Begg and Mouslopoulou, 2010). This explanation is consistent with the displacement profiles in Fig. 6b, which show that fault scarps (black triangles) are typically observed towards throw maxima and the southwest ends of faults where topography is most subdued.

In order to assess the timing of faulting in the rift since ca. 5.5 Ma, the accumulation of displacement on each of the 47 faults is plotted as a function of time (Fig. 5a). Cumulative fault displacements, measured across seismic reflectors of 0.5, 2.7, 3, 3.6 and 5.5 Ma in age, range from 20 m to ca. 1500 m (Figs. 3a and 5a). The majority of the rift faults, including the active faults, commenced their present phase of activity at about 3.6 Ma, with little or no fault growth between 5.5 and 3.6 Ma (Fig. 5a).

The relations between fault length and total displacement are further explored by plotting the maximum vertical displacement (or displacement rate) on each buried fault since 3.6 Ma against its fault length (Fig. 5b). These variables have a positive relationship similar to other fault systems globally, in which the longer faults move faster than the shorter faults (Nicol et al., 1997, 2005a; Wesnousky, 1999; Walsh et al., 2002; Mouslopoulou et al., 2009). In Fig. 5, we distinguish active faults (with surface traces and with post-0.5 Ma displacement but no surface traces) from faults which appear to be inactive (black circles) within the resolution of the data. The plots confirm that the majority of active faults tend to have the largest maximum throws and highest million-year displacement rates (Fig. 5b and c). The similar distributions of active faults in Fig. 5b and c are to be expected given that the displacement rates were determined using the maximum throws. The tendency of the active faults to have the largest lengths and displacements in the system could indicate strain localization onto the largest faults in the rift with increasing system maturity (see Meyer et al., 2002; Walsh et al., 2003). It is also possible that the predominance of relatively high displacement rate faults in Fig. 5c may reflect the fact that slower moving active faults are generally below the detection limit for active faults. In Fig. 5c, for example, the grey horizontal line defines the resolution limit for a 1 m high fault scarp on the ~27 kyr surface.

Table 1
Attributes of the active faults in the Taranaki Rift (those which have resolvable fault scarps at ground surface). In all likelihood there are many other active faults which are not marked by surface traces.

Fault ID	Dip (°)	Active-fault trace (km)	Subsurface fault trace (km)	No of EQ's (over time period)	Holocene displacement rate (~10 kyr)	Long-term displacement rate (3.6 Ma)	Observed RI[a] (kyr)	Calculated RI[b] (kyr)
Rahotu	85 SE	1.4	20	2 (14 kyr)	0.16	0.11	6.70	9.30
Oaonui	80–90 NW	13.2	25	4 (24 kyr)	0.11	0.08	6.90	16.47
Kina	80–85 NW	4	30	3 (7.8 kyr)	0.40	0.18	2.60	8.52
Ihaia	60–80 NW	5	28	4 (4.5 kyr)	0.35	0.10	1.90	14.44
Kiri	80–90 NW	6	30	5 (3 kyr)	1.67	0.03	1.10	49.08
Pihama	80–85 NW	4	25	5 (27 kyr)	0.21	0.10	4.8	12.50

[a] Average earthquake recurrence interval observed in the trenches.
[b] Calculated from Wells and Coppersmith (1994) equation: $RI = (5 \times 10^{-5})L/DR$, where DR = average displacement rate since 3.6 Ma and L = subsurface fault length.

The resolved active faults tend to be above this line while many of the faults below the line would not be identified as active even if they were. Therefore, the absence of a systematic displacement rate-length scaling relationship for active faults in Fig. 5c may simply reflect the incompleteness of the data.

Finally, in order to chart the distribution of throw along each active fault over different periods of time, we have utilised subsurface seismic-reflection data to produce along-strike displacement profiles for four time-windows (0–2.7 Ma, 0–3 Ma, 0–3.6 Ma and 0–5.5 Ma) (Fig. 6a). The shape and spatial extent of the profiles appear to persist through time, which reinforces the notion that faults establish their length rapidly and subsequently grow by accumulating displacement through successive earthquakes (Walsh et al., 2002; Nicol et al., 2005b). In order to examine the displacement distribution over much shorter timescales, displacements along active-fault traces have been normalised and plotted against the long-term displacement profiles (Fig. 6b). These graphs show a remarkable similarity between profiles produced by 4–5 earthquakes and by 100's or 1000's of earthquakes, indicating that the shape of profiles is independent of the time-window of observation. Based on these data (Fig. 6b) we infer that co-seismic slip distributions are also generally similar to the long-term displacement patterns for those earthquakes that rupture the entire fault length. It is noted however that trench data do not permit surface-rupturing earthquakes with throws <0.2 m to be routinely resolved and therefore provide little or no information on smaller events (e.g., <M5.5), some of which may only rupture part of a fault surface.

4. Fault displacement rates

Fault displacement rates vary spatially and temporally in the Taranaki Rift. Fig. 7a illustrates the throw accumulation on each of the six active faults for up to 80 kyr. Changes in displacements between data points on each curve are inferred to result from at least one surface-rupturing earthquake. The slopes on the growth curves in Fig. 7a suggest that the rates at which earthquakes were accommodated in the system during the last 27 kyr varied significantly between faults. This variability exceeds one order of magnitude, i.e. from ca. <0.1 mm/yr on the Oaonui Fault to ca. 1.6 mm/yr on the Kiri Fault. Further examination of the curves in Fig. 7a shows that, in addition to rates being variable between faults, displacement rates also appear to vary with time on some faults. The Pihama Fault, for example, has undergone two periods of accelerated growth (22–27 and 0–13 kyr) which are separated by a ~10 kyr time interval of relative seismic quiescence. This temporal variability in the short-term displacement rates may reflect temporal clustering of earthquakes arising from stress transfer and interaction between faults (Stein et al., 1997; Nicol et al., 2006; Dolan et al., 2007).

Table 2
Attributes of subsurface faulting in the Taranaki Rift.

Number of flts	47
Ave. strike	N40 E
Ave. dip	60–80°
Length	2–30 km
Displacements	20–1400 m
Displ. rate	0.005–0.4 mm/yr
Recur. interval	2.8–74.9 kyr

Million-year displacement rates range from ca. 0.025 to 0.2 mm/yr. On individual faults these rates varied temporally since the inception of faulting at ~3.6 Ma (Fig. 7b). The majority of active faults in the rift initiated their growth (between 3.6 and 2.7 Ma) at rates that are up to four times faster than their subsequent growth rates. This period of faster activity is also observed on the offshore Cape Egmont Fault (Fig. 2) and has been attributed to regional changes in strain rates arising from plate-boundary scale processes (Nicol et al., 2005a). Therefore, the increase in displacements rates on most onshore faults in the rift for this ~1 Ma time interval is inferred to reflect a period of increased regional strain rates.

Comparison of tens of thousand years (<27 kyr) and million-year (e.g., averaged since 3.6 Ma) displacement rates for each fault with a resolvable active trace suggests that they all accrued displacement more rapidly in the short-term (Fig. 8a). The majority of faults with active traces accumulated displacements between two and four times faster during 0–27 kyr than averaged since 3.6 Ma (Fig. 7, Table 1). The Kiri Fault, which has the lowest displacement rate averaged since the inception of faulting (ca. 3.6 Ma), has moved up to 50 times faster recently compared to its million-year old rate (Fig. 8a). By contrast, the Oaonui Fault, which appears to be the slowest moving fault in the system during the last 27 kyr, has an average long-term rate at about 72% of the short-term rate (Figs. 7b and 8a).

The increase in displacement rates on active faults during the last 27 kyr could be due to increasing single-event displacement and/or to decreasing recurrence intervals between events. The million-year displacement profiles suggest that fault lengths have not changed significantly since 5.5 Ma (Fig. 6a) and, as maximum earthquake-slip increases proportionally with length (e.g., Wells and Coppersmith, 1994; Pavlides and Caputo, 2004; Villamor et al., 2007), maximum slip has probably also remained constant. Therefore, the increase in short-term rate for active faults with observable scarps cannot be attributed to fault propagation with associated increases in maximum single-event displacement. Comparison of observed (in the trenches) recurrence intervals with estimates based on the long-term average suggests that a decrease in recurrence intervals may contribute to the increase in rates (Fig. 8b). Estimates of the long-term average recurrence interval were calculated from equation $RI = (5 \times 10^{-5})L/DR$ of Wells and Coppersmith (1994), assuming characteristic slip per event (DR = average displacement rate since 3.6 Ma; L = subsurface fault

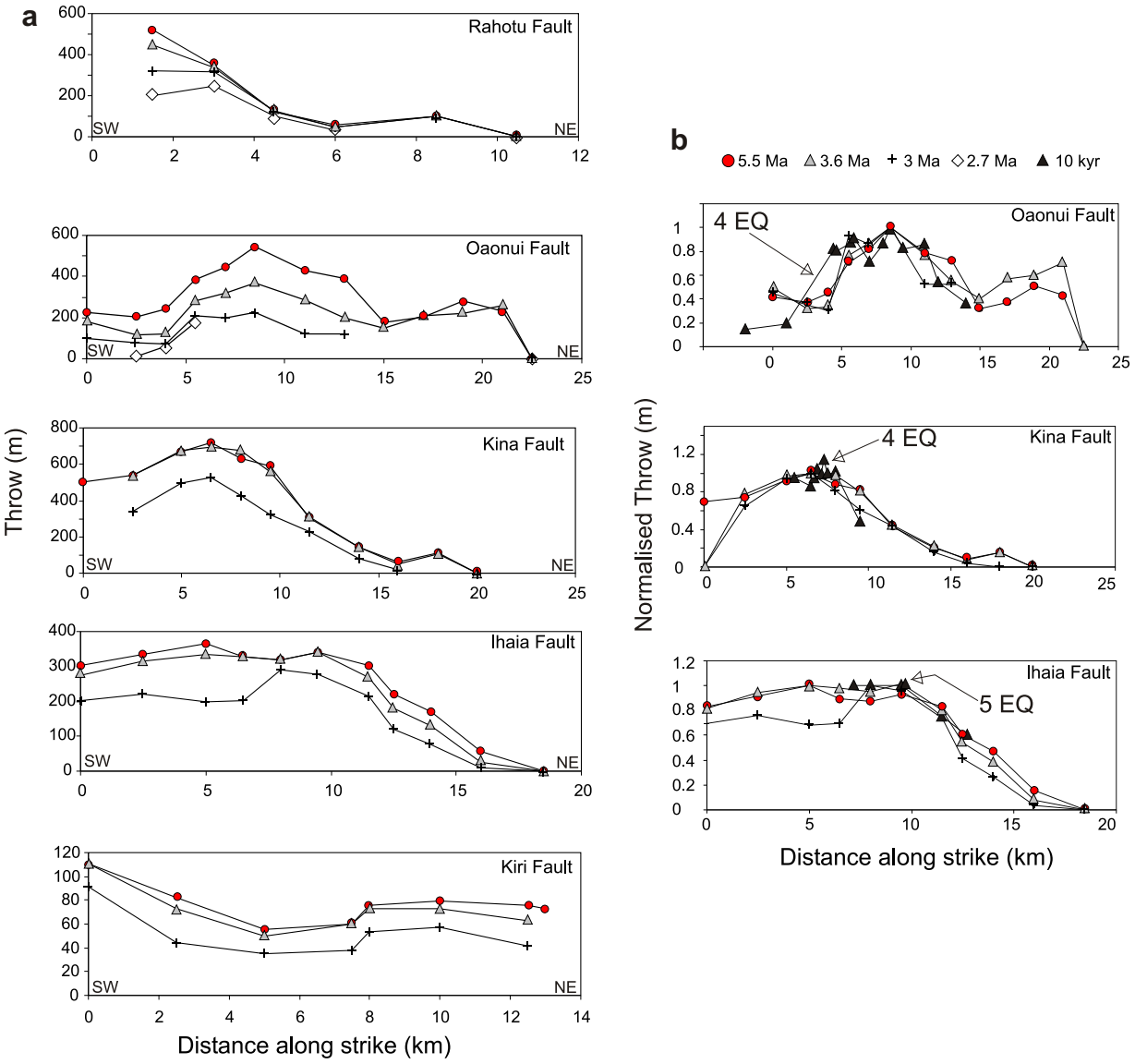

Fig. 6. a) Vertical displacement (i.e. throw) profiles for time-periods of 0–2.7, 0–3, 0–3.6 and 0–5.5 Ma on five of the active faults in the Taranaki Rift. b) Normalised Holocene (black triangles) and million-year displacement profiles plotted as a function of strike distance along three of the active rift faults. Normalisation per time interval is achieved by dividing each along-strike displacement with the largest displacement recorded on this specific fault. Arrows and associated labels indicate the number of successive paleo-earthquakes that generated the measured Holocene (i.e. 10 kyr) profile. Million-year old profiles in (a) and (b) were generated by 100's to 1000's of earthquakes.

length). Data show that for up to 27 kyr, earthquakes have ruptured the ground surface in the rift much more frequently than the estimates based on the million-year displacements, displacement rates and lengths (Fig. 8b). Indeed, trench data suggest that the observed earthquakes have occurred on the active faults in the system up to 30 times (see Kiri Fault in Fig. 8b) more frequently than would be inferred from long-term fault displacement rates.

Increased displacement rates on some rift faults during the last 27 kyr could reflect regional changes in the rates of extension and/or sampling bias. Potential increases in extension rates across the rift could result from: a) regional readjustments in the plate-boundary kinematics (e.g., changes in the relative plate motions or in the rates of subducting slab), and/or b) increases in the volcanic activity and dike intrusion within the rift, which could locally increase stresses and trigger earthquakes (Sherburn and White, 2006). Comparison of geodetic (<15 years) and geological (<2 Ma) strain measurements across the Hikurangi margin (Nicol and Wallace, 2007), suggests that rates of extension in the Taranaki region have not changed significantly since 2 Ma. Therefore, we infer that elevated Holocene rates did not result from regional changes in strain rates. In addition, there is presently little evidence to support the idea that volcanic eruptions are capable of influencing the growth of faults on timescales of thousands of years or more (Townsend et al., 2010; Seebeck and Nicol, 2009).

Our favoured explanation for the elevated short-term displacement rates is that they developed due to temporal clustering of earthquakes on individual faults in combination with a sampling bias towards faults with the shortest recurrence intervals during the Holocene (see Nicol et al., 2009). Earthquake clustering has been documented on many faults globally (Coppersmith, 1989; Sieh et al., 1989; Kagan and Jackson, 1991; Grant and Sieh, 1994; Marco et al., 1996; Rockwell et al. 2000; Dawson et al., 2003; Weldon et al., 2004; Nicol et al., 2006), and may chiefly result from fault interactions coupled with the

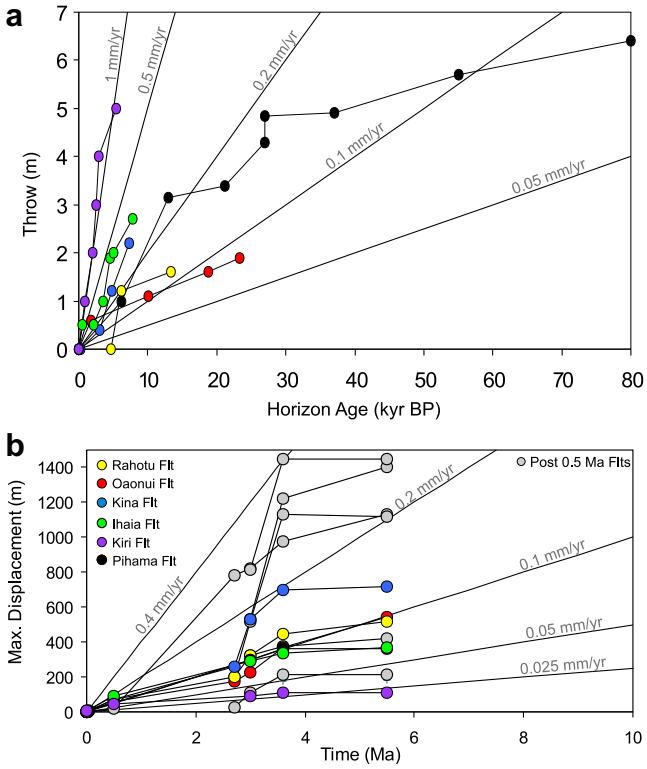

Fig. 7. Throw accumulation on the six active faults with surface traces in the Taranaki Rift over (a) short (<27 kyr) and (b) million-year (0–5.5 Ma) timescales. The long-term growth of the seven faults that displace the 0.5 Ma horizon but do not have a resolvable active trace is also illustrated by grey filled circles.

inherent complexity of earthquake occurrence on faults (Nicol et al., 2006; Mouslopoulou et al., 2009). Sampling bias is also generated by our tendency to mainly sample those faults which are better preserved in the landscape, often through impressive fault scarps (Nicol et al., 2009). These faults are likely to be those which have accommodated a series of successive earthquakes (and slip) recently (e.g. during the Holocene). This view is supported by seismic-reflection lines which show that, in addition to the six ground-rupturing faults, there are at least a further seven faults, including the larger faults in the system, that reach within ~50 m of the modern ground surface and are probably active (i.e. capable of producing future ground-rupturing earthquakes) (Fig. 3b).

For these additional seven active faults, long-term displacement rates are greater than Holocene rates by up to a factor of five (Fig. 8a). Thus, faults with increased and decreased displacement rates in the Holocene could be present in approximately equal proportions. As a result of these temporal rate changes, the sums of long-term rates on all faults in the system and Holocene rates on the 13 active faults identified are similar (i.e. long-term 3.4 ± 0.5 mm/yr and Holocene 3.1 ± 0.5 mm/yr). This similarity in the sum of the rates over each time interval supports the view that the regional rates of extension may not have changed, and that the temporal clustering of earthquakes reflects migration of the locus of fault activity from one fault to another, as proposed for the Basin and Range fault system (USA) by Wallace (1987). An important consequence of this migration is that faults which are currently in a relatively quiescent phase of earthquake activity may in the next 10 kyr, for example, become relatively active. Earthquake hazard analysis must take account of these relatively quiescent faults.

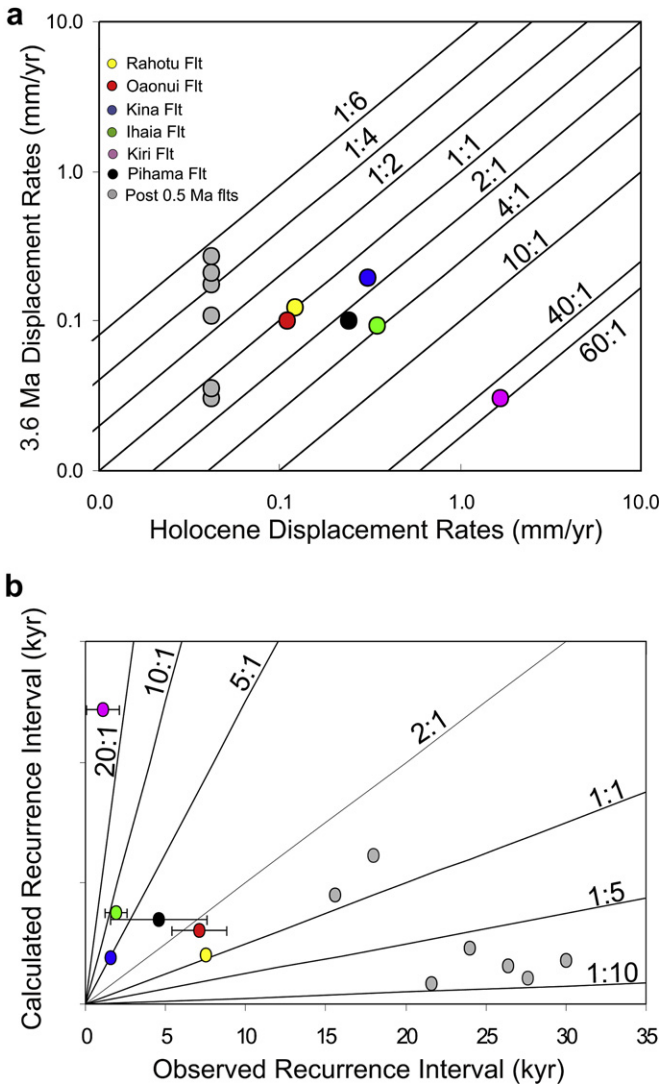

Fig. 8. (a) Log–log plot illustrating the relationship between post-27 kyr and 3.6 Ma displacement rates for each fault in the rift that ruptured the ground surface and the 0.5 Ma horizon. Maximum post-27 kyr rates for the latter faults are calculated assuming that they have displaced the ground surface by 1 m (maximum possible sub-resolution throw) divided by the maximum age of the ground surface (i.e., 27 kyr). (b) Plot comparing the observed (in trenches) earthquake recurrence interval with that calculated for each active fault in the system based on the Wells and Coppersmith (1994) relation. Faults that displace the 0.5 Ma horizon are also included for comparison (grey filled circles).

5. Earthquakes and seismic hazard

Data used to determine paleoearthquake histories and the resulting earthquake hazards are typically incomplete and subject to a number of sampling biases. In the case of the Taranaki Rift ≤50% of the active faults have surface traces ($N = 6$) and, until recently (Townsend et al., 2008) only one active fault was identified in the area of study. One consequence of this incompleteness is that the number of potential earthquake sources may be significantly higher than is represented in seismic hazard models. As a result, some future earthquakes will occur on faults that were not previously known to be active. This point is illustrated by the September 4th 2010, M7.1 and February 22nd 2011, M6.3 Christchurch earthquakes in New Zealand, both of which caused significant damage and occurred on previously unknown active faults (Allen et al., 2010; Van Dissen et al., 2011).

Faults most susceptible to this sampling bias are those with low Holocene displacement rates that do not produce resolvable surface traces. Because these sub-resolution faults may have important repercussions for seismic hazard, as was the case in Christchurch, attempts should be made to incorporate them into seismic hazard models. In regions such as the Taranaki Rift, where extensive subsurface seismic-reflection data are available, it may be possible to identify potentially active faults (as we have done here, see Fig. 3a) and input these into seismic hazard models. In such a case robust criteria must be established for identifying active faults that do not break the ground surface. In the Taranaki Rift, faults that displace the 0.5 Ma horizon, and most of which appear to displace rocks within 50 m of the ground surface, are considered active.

Displacement rate is the most widely used measure of earthquake activity. It is clear from this and other studies (e.g., Wallace, 1987; Coppersmith, 1989; Sieh et al., 1989; Kagan and Jackson, 1991; Grant and Sieh, 1994; Marco et al., 1996; Rockwell et al. 2000; Dawson et al., 2003; Weldon et al., 2004; Nicol et al., 2006; Mouslopoulou et al., 2009), that displacement rates on individual faults vary temporally. For the purposes of earthquake hazard assessment, displacement rates resulting from the most recent two to five paleoearthquakes are typically treated as representative of future rates of activity. However, given the variability in displacement rates arising from earthquake clustering, these short-term rates could underestimate or overestimate future rates. By contrast, displacement rates on active faults without active traces will be underestimated. One means of rectifying this is to assign long-term average displacement rates to faults with no resolvable active trace. It should be noted, however, that this approach will tend to overestimate the realistic short-term rates in circumstances where these faults are experiencing a period of relative earthquake quiescence.

It is widely acknowledged that fault-rupture lengths from paleoearthquake scarps are often underestimates of the true rupture length (Wells and Coppersmith, 1994; Biasi and Weldon, 2006; Wesnousky, 2008; Falcucci et al., 2009). This is certainly true of the Taranaki Rift dataset and may lead to underestimation of the magnitude of surface-rupturing earthquakes (see Wells and Coppersmith, 1994). For this reason, in Taranaki, we advocate using the subsurface fault length determined from seismic-reflection data.

Overall, this study draws on the potential incompleteness associated with fault data that span short (<27 kyr) timescales and highlights the significance of using, where possible, seismic-reflection data along with the paleoseismic methods. Seismic-reflection data may effectively complement outcrop (or near-surface) measurements by helping in the identification of buried faults, improving estimates of the maximum fault-rupture lengths and calibrating short-term estimates of displacement accumulation on faults. Combined use of seismic-reflection and paleoseismic data will lead to better estimates of the seismic hazard associated with a particular seismic source. Similarly, in offshore regions the combined analysis of bathymetric and seismic-reflection data may also be useful.

6. Conclusions

Over millions of years, active faults grow relatively uniformly to reach kilometre-scale cumulative displacements due to recurring large-magnitude earthquakes. However, over increasingly shorter timescales, displacement rates on many individual faults become increasingly irregular, reflecting a combination of variable earthquake behaviour (i.e. recurrence interval and single-event displacement) and incomplete sampling. The relations between fault displacement rates on short (<27 kyr) and long (>1 Ma) timescales in the Taranaki Rift, New Zealand, have been examined using high-quality trench and coastal outcrop data together with deep (<5 km) onshore seismic-reflection lines. Comparison of paleoearthquake and million-year displacement rates suggests that the short-term rates on individual faults significantly fluctuate around the long-term averages. These rate changes primarily reflect the natural variability of earthquake recurrence intervals, which we attribute to arise from the nonlinearity of the earthquake process, fault interactions, and associated migration of earthquake activity within the rift on selected faults. The shapes of along-strike displacement profiles for each time interval are comparable, suggesting that fault lengths, maximum single-event displacements and maximum-earthquake magnitudes have not changed over the last 3.6 Ma, and are unlikely to contribute to temporal variations in displacement rates. Surface fault traces have been recognised along ≤50% of their lengths and for <50% of the active faults. Integration of seismic reflection with paleoseismic data provides a basis for identifying active faults not observed at the ground surface, estimating maximum fault-rupture lengths, inferring maximum short-term displacement rates and improving earthquake hazard assessment.

Acknowledgements

This research was funded by an IIF Marie Curie Fellowship of the European Community's 7th Framework Program under contract no. PIIF-GA-2009-235931 and an IRCSET (Irish Research Council for Science, Engineering and Technology) Embark Initiative Postdoctoral Fellowship. We thank the Petroleum Geoscience Department of GNS Science for providing access to the seismic-reflection profiles. D. Heron, D. Beetham, B. Lukovic, H. Seebeck, R. Carne, P. Partsinevelos, S. Bogiatzi, S. Tsiligianni are sincerely acknowledged for assisting during fault trenching. Richard Norris is thanked for a thorough and constructive review and the Editor (T. Blenkinsop) is thanked for efficiently handling this article.

References

Allen, J., Bradley, B., Green, R.A., Orense, R., Wotherspoon, L., Ashford, S., Cox, B., Hutchinson, T., Pender, M., Bowman, E., Cubrinovski, M., Kavasanjian, E., Quigley, M., 2010. Geotechnical reconnaissance of the 2010 Darfield (Canterbury) earthquake. Bulletin of the New Zealand Society for Earthquake Engineering 43, 243–320.

Alloway, B.V., McComb, P., Neall, V., Vucetich, C., Gibb, J., Sherburn, S., Stirling, M.W., 2005. Stratigraphy, age, and correlation of voluminous debris-avalanche events from an ancestral Egmont Volcano: implications for coastal plain construction and regional hazard assessment. Journal of the Royal Society of New Zealand 35, 229–267.

Begg, J.G., Mouslopoulou, V., 2010. Analysis of late Holocene faulting within an active rift using lidar, Taupo Rift, New Zealand. Journal of Volcanology and Geothermal Research 190, 152–167.

Biasi, G.P., Weldon, R.J., 2006. Estimating surface rupture length and magnitude of paleoearthquakes from point measurements of rupture displacement. Bulletin of the Seismological Society of America 96, 1612–1623. doi:10.1785/0120040172.

Coppersmith, K.J., 1989. On spatial and temporal clustering of paleoseismic events. Seismological Research Letters 59, 299–330.

Cowie, P.A., Scholz, C.H., 1992. Growth of faults by accumulation of seismic slip. Journal of Geophysical Research 97, 11085–11095.

Dawson, T.E., McGill, S.F., Rockwell, T.K., 2003. Irregular recurrence of paleoearthquakes along the central Garlock fault near El Paso Peaks, California. Journal of Geophysical Research 108 (B7), 2356. doi:10.1029/2001JB001744.

Dieterich, J., 1994. A constitutive law for rate of earthquake production and its application to earthquake clustering. Journal of Geophysical Research 99 (B2), 2601–2618.

Dolan, J.F., Bowman, D.D., Sammis, C.G., 2007. Long-range and long-term fault interactions in Southern California. Geology 35, 855–858. doi:10.1130/G23789A.1.

Downes, G.L., 1995. Atlas of isoseismal maps of New Zealand earthquakes. In: Institute of Geological & Nuclear Sciences Monograph 11. Institute of Geological & Nuclear Sciences, Lower Hutt, 304 p.

Falcucci, E., Gori, S., Peronace, E., Fubelli, G., Moro, M., Saroli, M., Giaccio, B., Messina, P., Naso, G., Scardia, G., Sposato, A., Voltaggio, M., Galli, P., Galadini, F., 2009. The Paganica fault and surface coseismic ruptures caused by the 6 April 2009 earthquake (L'Aquila, Central Italy). Seismological Research Letters 80, 940–950.

Giba, M., 2010. The evolution of tertiary normal faults in the Taranaki Basin, New Zealand. Unpublished PhD thesis, University College Dublin, Dublin, Ireland.

Giba, M., Nicol, A., Walsh, J.J., 2010. Evolution of faulting and volcanism in a back-arc basin and its implications for subduction processes. Tectonics 29. doi:10.1029/2009TC002634.

Grant, L.B., Sieh, K., 1994. Paleoseismic evidence for clustered earthquakes on the San Andreas fault in the Carrizo Plain, California. Journal of Geophysical Research 99, 6819–6841.

Hull, A.G., 1994. Past earthquake timing and magnitude along the Inglewood fault, Taranaki, New Zealand. Bulletin of the New Zealand National Society for Earthquake Engineering 27, 155–162.

Kagan, Y.Y., Jackson, D.D., 1991. Worldwide doublets of large shallow earthquakes. Bulletin of the Seismological Society of America 89, 1147–1155.

Kagan, Y.Y., 1994. Observational evidence for earthquakes as a nonlinear dynamic process. Physica D 77, 160–192.

King, P.R., Thrasher, G.P., 1996. Cretaceous and Cenozoic geology and petroleum systems of the Taranaki Basin, New Zealand. In: Institute of Geological & Nuclear Sciences Monograph 13, 243 p.

Li, Q., Liu, M., Stein, S., 2009. Spatiotemporal complexity of continental intraplate seismicity: insights from geodynamic modeling and implications for seismic hazard estimation. Bulletin of the Seismological Society of America 99, 52–60. doi:10.1785/0120080005.

Lindvall, S., Rockwell, T., Hudnut, K., 1989. Evidence for prehistoric earthquakes on the Superstition Hills fault from offset geomorphic features. Bulletin of the Seismological Society of America 79, 342–361.

McCalpin, J.P., 2009. Paleoseismology, second ed. Academic Press, ISBN 0123735769. ISBN: 978-0123735768.

Marco, S., Stein, M., Agnon, A., 1996. Long-term earthquake clustering: a 50 000-year paleoseismic record in Dead Sea Graben. Journal of Geophysical Research 101, 6179–6191.

Meyer, V., Nicol, A., Childs, C., Walsh, J.J., Watterson, J., 2002. Progressive localization of strain during the evolution of a normal fault system in the Timor Sea. Journal of Structural Geology 24, 1215–1231.

Mouslopoulou, V., Walsh, J.J., Nicol, A., 2009. Fault displacement rates on a range of timescales. Earth and Planetary Science Letters 278, 186–197.

Mouslopoulou, V., Hristopulos, D., 2011. Patterns of tectonic fault interactions captured through variogram analyses of microearthquakes. Journal of Geophysical Research 116, B07305. doi:10.1029/2010JB007804.

Neall, V.E., Alloway, B.V., 2004. Quaternary Geological Map of Taranaki, New Zealand, 1:100,000. Institute of Natural Resources – Massey University, Soil & Earth Sciences Occasional Publication No. 4.

Nicol, A., Walsh, J., Watterson, J., Underhill, J.R., 1997. Displacement rates of normal faults. Nature 390, 157–159.

Nicol, A., Walsh, J.J., Berryman, K., Nodder, S., 2005a. Growth of a normal fault by the accumulation of slip over millions of years. Journal of Structural Geology 27, 327–342.

Nicol, A., Walsh, J.J., Manzocchi, T., Morewood, N., 2005b. Displacement rates and average earthquake recurrence intervals on normal faults. Journal of Structural Geology 27, 541–551.

Nicol, A., Walsh, J.J., Berryman, K., Villamor, P., 2006. Interdependence of fault displacement rates and paleoearthquakes in an active rift. Geology 34, 865–868.

Nicol, A., Mazengarb, C., Chanier, F., Rait, G., Uruski, C., Wallace, L., 2007. Tectonic evolution of the active Hikurangi subduction margin, New Zealand, since the Oligocene. Tectonics 26, TC4002. doi:10.1029/2006TC002090.

Nicol, A., Wallace, L., 2007. Temporal stability of deformation rates: comparison of geological and geodetic observations, Hikurangi Margin, New Zealand. Earth and Planetary Science Letters 258, 397–413.

Nicol, A., Walsh, J.J., Mouslopoulou, V., Villamor, P., 2009. Earthquake histories and Holocene acceleration of fault displacement rates. Geology 37, 911–914.

Palumbo, L., Benedetti, L., Bourles, D., Cinque, A., Finkel, R., 2004. Slip history of the magnolia fault (Apennines, Central Italy) from 36 Cl surface exposure dating: evidence for strong earthquakes over the Holocene. Earth and Planetary Science Letters 225, 163–176.

Pavlides, S., Caputo, R., 2004. Magnitude versus faults' surface parameters: quantitative relationships from the Aegean. Tectonophysics 380, 159–188.

Reyners, M., 1989. New seismicity 1964–87: an interpretation. New Zealand Journal of Geology and Geophysics 32, 307–315.

Robinson, R., Calhaem, I.M., Thomson, A.A., 1976. The Opunake, New Zealand, earthquake of 5 November 1974. New Zealand Journal of Geology and Geophysics 19, 335–345.

Rockwell, T.K., Lindvall, S., Herzberg, M., Murbach, D., Dawson, T., Berger, G., 2000. Paleoseismology of the Johnson Valley, Kickapoo, and Homestead Valley faults: clustering of earthquakes in the Eastern California shear zone. Bulletin of the Seismological Society of America 90, 1200–1236.

Schlagenhauf, A., Manighetti, I., Benedetti, L., Gaudemer, Y., Finkel, R., Malavieille, J., Pou, K., 2011. Earthquake supercycles in Central Italy, inferred from ^{36}Cl exposure dating. Earth and Planetary Science Letters 307, 487–500.

Schwartz, D.P., Coppersmith, K.J., 1984. Fault behavior and characteristic earthquakes: examples from the Wasatch and San Andreas fault zones. Journal of Geophysical Research 89, 5681–5698.

Seebeck, H., Nicol, A., 2009. Dike intrusion and displacement accumulation at the intersection of the Okataina Volcanic Centre and Paeroa Fault zone, New Zealand. Tectonophysics 475 (3–4), 575–685. doi:10.1016/j.tecto.2009.07.009.

Sherburn, S., White, R.S., 2005. Crustal seismicity in Taranaki, New Zealand using accurate hypocentres from a dense network. Geophysical Journal International 162, 494–506.

Sherburn, S., White, R.S., 2006. Tectonics of the Taranaki region, New Zealand: earthquake focal mechanisms and stress axes. New Zealand Journal of Geology and Geophysics 49, 269–279.

Sieh, K., Stuiver, M., Brillinger, D., 1989. A more precise chronology of earthquakes produced by the San Andreas fault in Southern California. Journal of Geophysical Research 94, 603–623.

Stein, R.S., King, G.C., Rundle, J.B., 1988. The growth of geological structures by repeated earthquakes. 2. Field examples of continental dip-slip faults. Journal of Geophysical Research 93, 13,319–13,331.

Stein, A., Barka, A., Dieterich, H., 1997. Progressive failure on the North Anatolian fault since 1939 by earthquake stress triggering. Geophysical Journal International 128, 594–604.

Townsend, D., Vonk, A.J., Kamp, P.J.J., 2008. Geology of the Taranaki area: scale 1:250,000 geological map. In: Institute of Geological & Nuclear Sciences 1:250,000 geological map 7. GNS Science, Lower Hutt. 77 p., 1 folded map.

Townsend, D., Nicol, A., Mouslopoulou, V., Begg, J.G., Beetham, R.D., Clark, D., Giba, M., Heron, D., Lukovic, B., McPherson, A., Seebeck, H., Walsh, J.J., 2010. Paleoearthquake histories across a normal fault system in the southwestern Taranaki Peninsula, New Zealand. New Zealand Journal of Geology and Geophysics 53, 1–20.

Van Dissen, R., Barrell, D., Litchfield, N., Villamor, P., Quigley, M., King, A., Furlong, K., Begg, J., Townsend, D., Mackenzie, H., Stahl, T., Noble, D., Duffy, B., Bilderback, E., Claridge, J., Klahn, A., Jongens, R., Cox, S., Langridge, R., Ries, W., Dhakal, R., Smith, A., Hornblow, S., Nicol, R., Pedley, K., Henham, H., Hunter, R., Zajac, A., Mote, T., 2011. Surface rupture displacement on the Greendale fault during the Mw 7.1 Darfield (Canterbury) earthquake, New Zealand, and its impact on man-made structures. In: Proceedings of the Ninth Pacific Conference on Earthquake Engineering 14–16 April, 2011, Auckland, New Zealand, Paper Number 186, 8 pp.

Villamor, P., Van Dissen, R.J., Alloway, B.V., Palmer, A.S., Litchfield, N.J., 2007. The Rangipo Fault, Taupo rift, New Zealand: an example of temporal slip-rate and single-event displacement variability in a volcanic environment. Bulletin of the Geological Society of America 119, 529–547.

Walcott, R.I., 1987. Geodetic strain and the deformational history of the North Island of New Zealand during the late Cenozoic. Philosophical Transactions of the Royal Society of London A321, 163–181.

Wallace, R.E., 1987. Grouping and migration of surface faulting and variations in slip rates on faults in the Great Basin Province. Bulletin of the Seismological Society of America 77, 868–876.

Wallace, L.M., Beavan, R.J., McCaffrey, R., Darby, D.J., 2004. Subduction zone coupling and tectonic block rotations in the North Island, New Zealand. Journal of Geophysical Research 109, B12406. doi:10.1029/2004JB003241.

Walsh, J.J., Watterson, J., 1988. Analysis of the relationship between the displacements and dimensions of faults. Journal of Structural Geology 10, 239–247.

Walsh, J.J., Nicol, A., Childs, C., 2002. An alternative model for the growth of faults. Journal of Structural Geology 24, 1669–1675.

Walsh, J.J, Childs, C., Imber, J., Manzocchi, T., Watterson, J., Nell, P.A.R., 2003. Strain localisation and population changes during fault system growth within the Inner Moray Firth, Northern North Sea. Journal of Structural Geology 25, 1897–1911.

Weldon, R., Scharer, K., Fumal, T., Biasi, G., 2004. Wrightwood and the earthquake cycle: what a long recurrence record tells us about how faults work. GSA Today 14 (9), 4–10.

Wells, D.L., Coppersmith, K.J., 1994. New empirical relationships among magnitude, rupture length, rupture width, rupture area and surface displacement. Bulletin of the Seismological Society of America 8, 974–1002.

Wesnousky, S.G., 1999. Crustal deformation processes and the stability of the Gutenberg–Richter relationship. Bulletin of the Seismological Society of America 89, 1131–1137.

Wesnousky, S.G., 2008. Displacement and geometrical characteristics of earthquake surface ruptures: issues and implications for seismic-hazard analysis and the process of earthquake rupture. Bulletin of the Seismological Society of America 98, e1609–e1632. doi:10.1785/0120070111.

Zoback, M.D., 2000. Strength of the San Andreas. Nature 405, 31–32.